# Probing the Dissolved Gas Concentration on the Electrode through Laser-Assisted Bubbles

*AUTHOR NAMES*

*Kota Ando,[a] Yoshiharu Uchimoto,[b] and Takashi Nakajima *[a]*

AUTHOR ADDRESS

[a] Institute of Advanced Energy, Kyoto University, Gokasho, Uji, Kyoto 611-0011, Japan

[b] Graduate School of Human and Environmental Studies, Kyoto University, Sakyo-ku, Kyoto 606-8501, Japan

ABSTRACT

We demonstrate that the irradiation of a single laser pulse onto the electrode assists the formation of bubbles, and this phenomenon can be conveniently used to probe the dissolved gas concentration on the electrode. The obtained concentrations agree well with the values inferred through linear extrapolation of gas concentration in proximity to the electrode to the electrode surface.

**Introduction**

Hydrogen evolution reaction (HER) through electrolysis of water draws a lot of attentions in recent years, because hydrogen is considered to be a promising candidate for the carbon-neutral fuel. To realize highly efficient production of hydrogen lots of efforts have been made from different aspects. Finding/developing efficient electrocatalysts is obviously an important issue.[1–7] Improving the detachment of bubbles from the electrode is also very important,[1,3,7] since the coverage of the electrode surface by evolved gas bubbles leads to the increase of ohmic resistance and hence reduces the efficiency of electrolysis. Such a thought leads to the studies on the effect of morphology and the wettability of electrodes.[1,2,7,8] Coalescence of bubbles can occur not only on the electrode but also in the bulk electrolyte[9–11] after their detachments from the electrode, which can cause the complexity in the transport dynamics.

Starting from the birth of bubbles upon nucleation the behavior of the bubbles during electrolysis is strongly dependent on the local concentration of dissolved gas, and the electrochemical method with a micro/nanoelectrode is known to be very powerful to probe not only the nucleation process[8,11–15] but also local concentration of the dissolved gas in proximity to the electrode.[16] It is, however, a one-site-at-one-time method, and repeated measurements are necessary for the mapping over some area.[17,18] Recently we have developed an optical image tracking technique to probe the growth process of individual bubbles in proximity to the electrode,[19] and successfully obtained the concentration of the dissolved gas as a function of distance from the electrode with a reasonable agreement with the one obtained by the electrochemical method.[16] The essential difference between the above two methods is that the electrochemical method works at the timing and area where there are no bubbles, while the optical method requires the presence of bubbles. In

other words the electrochemical method works well under the very low to low current density while the optical method works well under the low to moderate current density. Since the optical method has a certain advantage that it is a multiple-site-at-one-time method and hence convenient to investigate the site-dependent behavior, exploring a way to extend the applicable current density range of optical method toward the lower current density where there are no or very few ordinary electrolysis bubbles is undoubtedly an important issue.

In this paper we develop a new technique to probe the dissolved gas concentration at the electrode. The key ingredient of the new technique is to introduce a single laser pulse and optically probe the growth of laser-assisted bubbles on the electrode. The advantage of introducing a laser pulse is that we can produce laser-assisted bubbles at the desired area on the electrode where there are very few (ideally no) ordinary electrolysis bubbles so that the image analysis of laser-assisted bubbles becomes simple.

**Experimental Section**

Figure 1 shows the experimental setup. It is similar to the setup we have developed in our recent study[19] with a very important difference that we now introduce a laser pulse to assist the formation of bubbles on the Ni wire electrode. As we explain later on, the home-made image analysis software is also newly developed to analyze the growth of laser-assisted bubbles sitting on the Ni wire electrode.

**Electrolysis cell.** We employ a Ni wire (99.9+%, $\phi$100 µm, Nilaco) and a Pt mesh (99.98%, 26 × 8 mm$^2$, $\phi$120 µm, 55 mesh/inch, Nilaco) as a working and counter electrodes, respectively. These electrodes are placed on a squared PTFE frame (40 × 40 mm$^2$ with a frame width of 5 mm), and immersed in 60 mL of 0.1 M KOH solution (FUJIFILM Wako Pure Chemical Co.) contained in an acrylic cuvette (50 × 50 × 50 mm$^3$). As shown in the left in Figure 1, the Ni wire is placed at a

lower position than the Pt mesh for the clear view of hydrogen bubbles on the Ni wire. The part of the Ni wire sticking out of the PTFE frame is covered by a heat-shrinkable tube so that the geometric surface area of the naked Ni wire is 100 μm × π × 3 cm = 0.094 $cm^2$. A reversible hydrogen electrode (RHE) is placed near the Ni wire, which serves as a reference electrode. All the three electrodes are connected to a potentiostat/galvanostat (HZ-7000, HOKUTO DENKO Co.). In this paper, we employ the constant-current mode for all the measurements, and the current is −2, −3, and −4 mA, which correspond to the current densities of −21, −32, and −43 $mA/cm^2$, respectively. Under these currents, the potential (vs RHE) of the Ni wire electrode is negative ~~by~~ and about −400 mV, which means that all the formed bubbles are hydrogen gases (Supporting Information, Figure S1a, S1b).
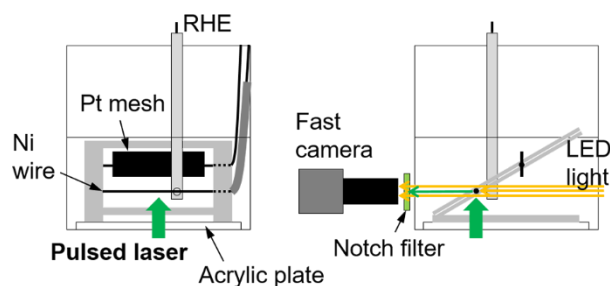


**Figure 1.** Experimental Setup. The laser beam diameter at the wire electrode is 7 mm to secure the uniform illumination of the observation area with a width of ~ 400 μm.

**Pulsed laser.** To assist the formation of bubbles on the wire electrode we introduce a nanosecond laser pulse. It is a second harmonic (532 nm) of the Q-switched Nd:YAG laser (GAIA2, Rayture Systems Co. Ltd., pulse duration 5 ns, maxium pulse energy 20 mJ at 532 nm, $M^2$~15). Due to the use of the wire electrode most of the ordinary electrolysis bubbles that have been formed on the wire electrode gradually slip on the curved electrode surface toward the top, and then leave the electrode. This is due to the buoyant force. To avoid the undesired light

scattering by those bubbles during the optical measurement we send the laser pulse from the bottom of the wire electrode as shown in Figure 1 where there are very few small bubbles prior to the laser pulse. The laser beam diameter at the wire electrode is 7 mm to secure the uniform illumination to the observation area with a width of ~400 μm. If the laser fluence is too low during electrolysis no additional bubbles are formed upon irradiation of a single laser pulse. Only if the laser fluence is sufficient at a given current additional bubbles (termed laser-assisted bubbles) are formed, and this occurs only once after each laser pulse. This is a very convenient situation to optically probe the bubble growth with a well-defined time zero until detachment. How many sites contribute to form laser-assisted bubbles upon laser irradiation depends on the laser fluence and of course employed current, and too much laser fluence (more than ~30 mJ/cm$^2$ for the case of −2 mA in this study) results in too many sites to form laser-assisted bubbles, which makes the detection of individual bubbles very difficult. After trial and error, we find that the laser fluence of ~14 mJ/ cm$^2$ (estimated from the pulse energy, 5.5 mJ, and the beam diameter, 7 mm) is appropriate for our electrolysis conditions. Note that this fluence is two orders of magnitude lower than the ablation threshold of Ni surface.[20] From the comparison of the scanning electron microscope (SEM) images of the electrode surface before and after the laser pulse we ensure that the electrode surface remains unaltered by the laser irradiation at this fluence (Supporting Information, Figure S2). After the electrolysis for ~100 s at the choice of current to be used for the following measurement, we turn on the laser at 1 Hz with the fluence of 14 mJ/cm$^2$ unless otherwise mentioned.

**High-speed camera.** Dynamics of the laser-assisted bubbles on the wire electrode are recorded with a high-speed camera (CP70-1-M-1000, Optronis GmbH, pixel size 6.6 μm and 4000 fps max for the resolution of 640×480 pixels) at the frame rate of 1000 per second under the LED

illumination (AS3000, As one Co.) through a notch filter (NF533-17, Thorlabs Co.) and a telecentric lens (ML 10×, Mitutoyo Co., NA 0.21, depth of focus 6.2 μm), which results in the field of view of 422 × 317 μm$^2$. The timing of the camera exposure and the laser pulse are synchronized through a delay generator (DG645, Stanford Research Systems), and the trigger signals are also stored in a PC via a voltage reader (NI 9215, National Instruments) so that we can identify at which frame of the movie the laser pulse is turned on.

**Image analysis.** For the image analysis of laser-assisted bubbles sitting on the electrode we develop a new program based on the image analysis VIs installed in NI LabVIEW (NI) (Supporting Information, Image analysis and Figure S3). Within a very short time after the birth, initially flat laser-assisted bubbles grow and become almost spherical on the electrode (Supporting Information, Movies S1-S3), and the newly developed program can analyze the one-piece image of "a bubble on the electrode" to extract the bubble growth rates through the following three steps (Supporting Information, Figure S3): (1) identify the lower-boundary of the electrode in the first frame (in which the laser pulse is turned on), and the bump's contour in the subsequent images, (2) evaluate the vertical distance of the respective bumps with respect to the lower-boundary of the electrode, and (3) determine the heights of the respective bumps through peak detection. By repeating steps (1)-(3) for all frames of the movies, we obtain the bubble growth rates. As we can see in the movies (Supporting Information, Movie S1-S3), the shape of the laser-assisted bubble is hemispherical up to the height of ~6 μm, but after that it becomes practically spherical with a very small contact area on the electrode surface. When the bubbles grow to the height of ~15.6 μm they start to detach from the electrode. Therefore, the most convenient size of the laser-assisted bubbles for the analysis of growth rate is 6–15 μm in terms of the bubble diameter.

**Results and discussion**

Figures 2a, 2b, Figures 2c, 2d, and Figures 2e, 2f show the formation of laser-assisted bubbles under the constant-current mode at −2, −3, and −4 mA, respectively. Figures 2a, 2c, and 2e are taken at 5 ms before the laser pulse, while Figures 2b, 2d, and 2f are taken at 20 ms after that. Clearly, the bubbles indicated by the yellow arrows in Figures 2b, 2d, and 2f are formed under the assistance of the laser pulse (see also Supporting Information, Movie S1-S3). Note that the laser pulses that are turned on at 0 ms are not visible in the movies (Supporting Information, Movies S1-S3) because they are completely blocked by the notch filter (Figure 1). As a general remark, we find that the laser-assisted bubbles are first observed at 2~3 ms after the laser pulse, and from the comparison of Figures 2b, 2d, and 2f (as well as Supporting Information, Movies S1-S3), we notice that the number of not only the ordinary electrolysis bubbles but also laser-assisted bubbles increases as the current increases (to the negative side). It is interesting to point out that the laser-assisted bubbles as well as the ordinary electrolysis bubbles are repeatedly produced at the same sites, i.e., sites A and B in Figure 2. For example, we focus on site A: at −2 mA no ordinary bubbles are formed at site A (Figure 2a), and it is only immediately after the laser pulse is irradiated when the laser-assisted bubble is formed at site A (Figure 2b). Similar is true when the current is increased to −3 mA (Figures 2c and 2d). At −4 mA, however, even an ordinary electrolysis bubble is observed at site A (Figure 2e). Those observations seem to imply that the laser pulse irradiation literally assist the formation of bubbles at site A. Qualitatively similar behaviors are observed for the ordinary electrolysis and laser-assisted bubbles at site B with a clear important difference that, at site B, even a laser-assisted bubble is not formed with this fluence when the current is −2 mA (Figure 2b). This difference suggests that, although both sites A and B are inactive at −2 mA without a laser pulse, site A is slightly more active than site B.
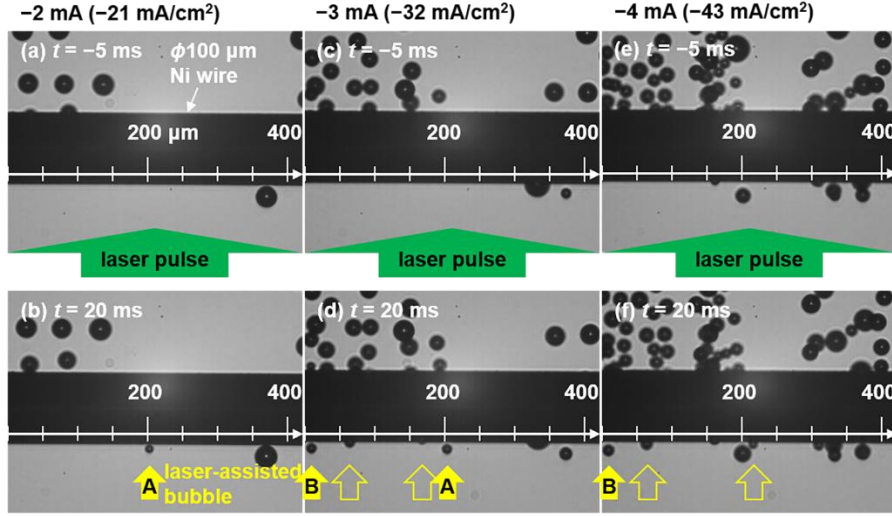
**Figure 2.** Formation of laser-assisted bubbles at the current of (a, b) −2, (c, d) −3, and (e, f) −4 mA, respectively. *t* is an elapsed time after the laser pulse. Bubbles are formed only on the irradiated side of the electrode, as shown by the yellow arrows. The laser fluence is 14 mJ/cm$^2$ for all graphs. Note that laser-assisted bubbles are not formed if the current is set zero.

What is the formation mechanism of laser-assisted bubbles? To find a hint of this question, we calculate the time evolution of the temperature of the electrode surface by referring to the discussion in the similar studies.[20,21] It is assumed that some of the laser energy absorbed by the Ni electrode surface is immediately converted to heat at the surface of the electrode, and the heat is diffused into the bulk of the electrode thorough a simple heat transport model. The temperature change, $\Delta T(t)$, of the surface can be estimated by the following equations[21]:

$$\Delta T(t) = 2 \times \frac{2(1-R)\,F/\tau}{\sqrt{\pi \kappa C_{\mathrm{p}} \rho}}\sqrt{t} \quad t \leq \tau \; \text{(Heating)} \qquad (1)$$

$$\Delta T(t) = 2 \times \frac{2(1-R)\,F/\tau}{\sqrt{\pi \kappa C_{\mathrm{p}} \rho}}\left[\sqrt{t} - \sqrt{t-\tau}\right] \quad t > \tau \; \text{(Cooling)} \qquad (2)$$

where $R$ is the reflectivity at the laser wavelength, $F$ and $\tau$ are the fluence and pulse duration of laser, while $\kappa$, $C_{\mathrm{p}}$, and $\rho$ are the thermal conductivity, heat capacity, and density of the electrode.

Here, we have already applied a factor of 2 to the above equation to take into account the Gaussian beam profile (because the fluence at the center of a Gaussian beam is about twice of the averaged fluence over the beam diameter). By substituting $F = 14$ mJ/cm$^2$, $\tau = 5$ ns, $R = 0.6$, $\kappa = 91$ W/(m·K), $C_p = 444$ J/(K·kg), and $\rho = 8900$ kg/m$^3$ [20] into eq 1 and 2, we obtain the time evolution of the temperature of the electrode surface, and the result is shown in Figure 3a. From this figure, we find that the maximum temperature increase of the electrode surface upon laser irradiation is about ~94 °C but it cools down to the room temperature within 1 μs. Since the rates of both bubble nucleation and hydrogen evolution reaction increase exponentially as a function of temperature, the temperature increase upon laser irradiation surely promotes the formation of bubble nucleus on the electrode surface. However, due to the rapid cooling the electrode is practically back to the room temperature when the optical measurement of bubbles starts at 1 μs after the laser irradiation. Moreover, as we show in Figure 3b, the Henry constant $k_H$ of hydrogen gas in pure water is nearly constant over the temperature range of 20~80 °C according to the literature.[22–24] From the above discussions, we can conclude the introduction of a laser pulse does not cause any problem to probe the dissolved gas concentration through the growth rates of laser-assisted bubbles. The remaining question is why the laser-assisted bubble formation is site-dependent on the electrode (Figure 2). We speculate that the geometry-dependent formation energy (in other words, stability) of bubble nucleus on the electrode may be the reason for this.
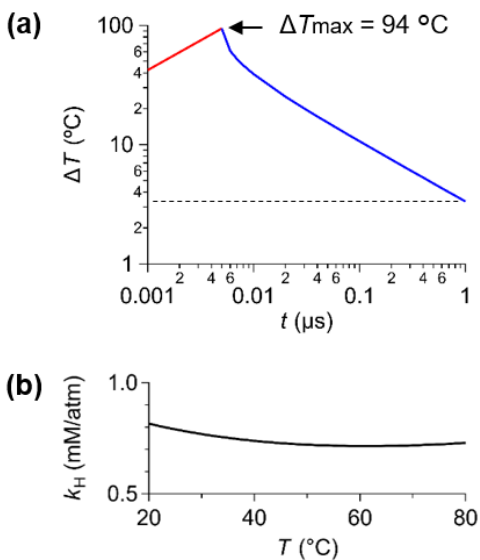
**Figure 3.** (a) Time evolution of the temperature increase $\Delta T$ of the electrode surface after the laser pulse at $t = 0$. Red and blue lines correspond to the heating and cooling processes, respectively. Within 1 µs after the laser irradiation, the temperature of the electrode surface is nearly back to the room temperature. (b) Variation of Henry constant $k_H$ for hydrogen gas in pure water as a function of temperaturecalculated by referring to the literature.[22]

For the laser-assisted technique we have described above to be reliable to probe the concentration of dissolved gas at the electrode we have to further ensure that the laser irradiation influences neither morphology of the electrode surface nor dissolved gas concentration. As for the former, we have already shown that the morphology of the electrode surface remains the same before and after laser irradiation (Supporting Information, Figure S2). As for the most direct proof of the latter, we have experimentally confirmed that the bubble growth speed remains practically the same for the laser fluence range of 14~22 mJ/cm², as shown by the horizontal yellow dashed line in Figure 4. Therefore, we can conclude that the concentration on the electrode can be reliably probed through laser-assisted bubbles.
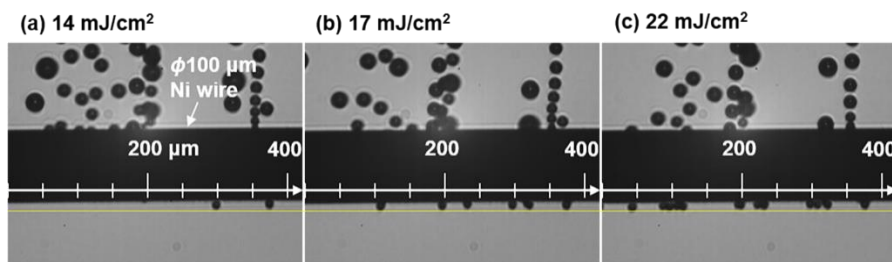
**Figure 4.** Laser-assisted bubbles at 20 ms after the laser pulse irradiated with the laser fluence of (a) 14, (b) 17, and (c) 22 mJ/cm$^2$ under the current of −2 mA. As the current density increases the number of laser-assisted bubbles also increases, but the growth speed remains the same (horizontal yellow lines).

Now, by performing the image analysis of bubbles (Supporting Information, Figure S3) for all frames of the movies (Supporting Information, Movies S1-S3) where representative frames are shown in Figures 2b, 2d, and 2f, we can extract the growth rates, $dR^2/dt$ with $R$ being the bubble radius (defined by half of the bubble height), of the laser-assisted bubbles on the electrode. Figure 5a shows the variation of the squared value of laser-assisted bubble radius, $R^2$, at sites A and B (Figure 2) as a function of elapsed time after the laser pulse. The slope of the curve is steeper for the higher current, and the bubble growth rate is approximately represented by a straight line, which agrees well with the theoretical prediction by the diffusion model without taking into account the Laplace pressure (Supporting Information, eq S5 with $\alpha = 1$). After $R^2$ grows beyond 60 μm$^2$ or equivalently $R > 7.8$ μm, the experimental data points deviate from the straight lines due to the bubble detachment from the wire electrode, for which our image analysis does not work. Note that the growth rates of the laser-assisted bubbles at sites A and B under the current of −3 mA are very similar (blue and green curves in Figure 5a), and this implies that the local concentrations of dissolved hydrogen around sites A and B are almost the same. Reproducibility of the bubble growth rate at the same site turns out to be very good, too, as shown in Figure 5b for

the five successive laser-assisted bubbles at site A under the current of −2 mA. Clearly, their behaviors are all very similar, and this demonstrates that the local concentration of dissolved hydrogen at site A remains nearly the same throughout the measurements. Performing the linear fittings to the five curves (in the range of 10 $\mu m^2 < R^2 < 60$ $\mu m^2$) shown in Figure 5b, we obtain the growth rate of 2.2 ± 0.1 $\mu m^2$/ms at site A under the current of −2 mA. Then, by substituting this growth rate, $dR^2/dt$, into the simplified Epstein Plessett equation[25] (Supporting Information, eq S5 with $\alpha = 1$), and solving it for the dissolved concentration of hydrogen gas, $C$, we finally obtain $C = 11.4 \pm 0.7$ mM, at site A under the current of −2 mA. We repeat the above procedures at site B under the different currents and without/with the Laplace pressure to solve the diffusion equation (Supporting Information, eq S5 with $\alpha = 1$ or 0.85 and Figure S4), and the results are summarized in Table 1. By taking into account the Laplace pressure the dissolved gas concentration turns out to be about 18% larger. The dissolved gas concentration increases approximately linearly as a function of current as shown in Figure 6. This is reasonable, because the flux of hydrogen molecules produced at the electrode is a linear function of the employed current. Concentrations, $C$, without taking into account the Laplace pressure, agree well with those obtained by the electochemical[16] and optical measurements in our recent study.[19] However , the values in Table 1 are a bit larger than those in our recent study. This is probably because the influence of convection is kept minimum around the inactive sites (such as sites A and B in Figure 2) where no bubbles are formed without the laser irradiation. It would be more clear if we are able to control the local roughness of the electrode surface and to compare the growth rates of laser-assisted bubbles at the site where ordinary electrolysis bubbles are repeatedly formed and that where they are not. The optical methods have been inapplicable to the site where there are no bubbles until now, but it becomes possible by the new technique we have developed in this study.

Since the optical method has a certain advantage that it is a multiple-site-at-one-time method and hence convenient to investigate the site-dependent behavior, the developed technique would be a new working horse to study the site-dependent bubble formation during electrolysis toward efficient hydrogen gas evolution.
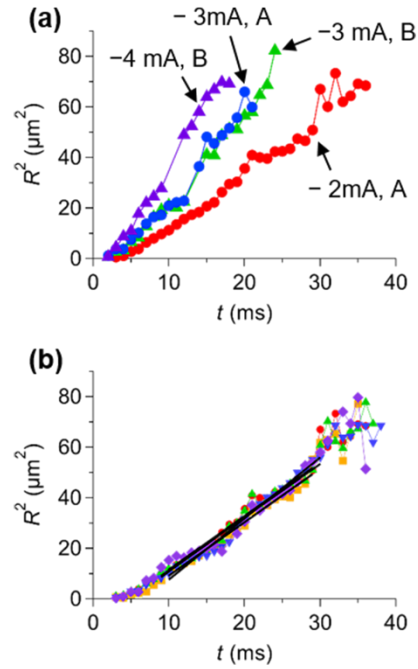


**Figure 5.** (a) Temporal variation of the square of the radius of laser-assisted bubbles at sites A and B (Figure 2) as a function of elapsed time after the laser pulse at different currents, −2, −3, and −4 mA. (b) Comparison of the temporal change of the squared radius, $R^2$, for the five successive laser-assisted bubbles at site A under the current of −2 mA.

**Table 1.** Growth rates, $dR^2/dt$, and concentrations of dissolved hydrogen gas, $C$, at sites A and B without/with taking into account the Laplace pressure (LP). The values after the plus-minus sign represent one standard deviation.

| current (mA) | site | $dR^2/dt$ ($\mu m^2$/ms) | $C$ (mM) without LP | $C$ (mM) with LP |
|---|---|---|---|---|
| −2 | A | 2.2±0.1 | 11.4±0.7 | 13.4±0.8 |

13

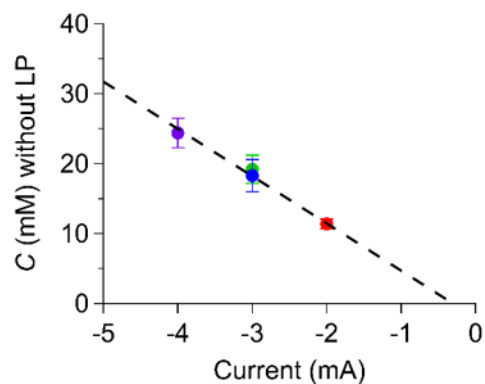| −3 | A | 3.6±0.5 | 18.3±2.3 | 21.5±2.7 |
| −3 | B | 3.8±0.4 | 19.2±2.0 | 22.6±2.3 |
| −4 | B | 4.9±0.4 | 24.4±2.1 | 28.8±2.5 |



**Figure 6.** (a) An increase of the dissolved gas concentration without taking into account Laplace pressure (LP) as a function of current.

## Conclusions

We have developed a new technique to probe the concentration of dissolved gas at the electrode through the optical detection of laser-assisted bubbles. Irradiation of a single laser pulse onto the electrode assists the formation of bubbles with a minimum temperature change of the irradiated part of the electrode and the surrounding electrolyte so that the bubble formation occurs without altering the concentration of dissolved hydrogen gas. From the image analysis of the movies we have obtained the growth rates of laser-assisted bubbles on the electrode. With the aid of diffusion model the growth rates have been recast into the local concentrations of the dissolved gas on the electrode. Unlike the electrochemical method which can probe only one site at one time, our optical method allows us to simultaneously measure the concentrations of multiple sites on the electrode

by the single measurement and hence within a few seconds. It can also be used as a very convenient technique to study the site-dependent bubble formation processes.

## ASSOCIATED CONTENT

SEM images of the electrode, image analysis, evaluation of dissolved gas concentration (PDF)

Formation of laser-assisted and ordinary bubbles at the current of -2 mA (AVI)

Formation of laser-assisted and ordinary bubbles at the current of -3 mA (AVI)

Formation of laser-assisted and ordinary bubbles at the current of -4 mA (AVI)

## AUTHOR INFORMATION

**Corresponding Author**

* Takashi Nakajima

nakajima@iae.kyoto-u.ac.jp

**Notes**

The authors declare no competing financial interest.

## REFERENCES

(1)     Lu, Z.; Zhu, W.; Yu, X.; Zhang, H.; Li, Y.; Sun, X.; Wang, X.; Wang, H.; Wang, J.; Luo, J.; Lei, X.; Jiang, L. Ultrahigh Hydrogen Evolution Performance of Under-Water

"Superaerophobic" MoS2 Nanostructured Electrodes. *Adv. Mater.* **2014**, *26* (17), 2683–2687. https://doi.org/10.1002/adma.201304759.

(2)     Chaudhari, N. K.; Jin, H.; Kim, B.; Lee, K. Nanostructured Materials on 3D Nickel Foam as Electrocatalysts for Water Splitting. *Nanoscale* **2017**, *9* (34), 12231–12247. https://doi.org/10.1039/c7nr04187j.

(3)     Darband, G. B.; Aliofkhazraei, M.; Shanmugam, S. Recent Advances in Methods and Technologies for Enhancing Bubble Detachment during Electrochemical Water Splitting. *Renew. Sustain. Energy Rev.* **2019**, *114* (July), 109300. https://doi.org/10.1016/j.rser.2019.109300.

(4)     Wang, H.; Gao, L. Recent Developments in Electrochemical Hydrogen Evolution Reaction. *Curr. Opin. Electrochem.* **2018**, *7*, 7–14. https://doi.org/10.1016/j.coelec.2017.10.010.

(5)     Dubouis, N.; Grimaud, A. The Hydrogen Evolution Reaction: From Material to Interfacial Descriptors. *Chem. Sci.* **2019**, *10* (40), 9165–9181. https://doi.org/10.1039/c9sc03831k.

(6)     McKone, J. R.; Marinescu, S. C.; Brunschwig, B. S.; Winkler, J. R.; Gray, H. B. Earth-Abundant Hydrogen Evolution Electrocatalysts. *Chem. Sci.* **2014**, *5* (3), 865–878. https://doi.org/10.1039/c3sc51711j.

(7)     Ahn, S. H.; Choi, I.; Park, H. Y.; Hwang, S. J.; Yoo, S. J.; Cho, E.; Kim, H. J.; Henkensmeier, D.; Nam, S. W.; Kim, S. K.; Jang, J. H. Effect of Morphology of Electrodeposited Ni Catalysts on the Behavior of Bubbles Generated during the Oxygen

Evolution Reaction in Alkaline Water Electrolysis. *Chem. Commun.* **2013**, *49* (81), 9323–9325. https://doi.org/10.1039/c3cc44891f.

(8)     Maheshwari, S.; Van Kruijsdijk, C.; Sanyal, S.; Harvey, A. D. Nucleation and Growth of a Nanobubble on Rough Surfaces. *Langmuir* **2020**, *36* (15), 4108–4115. https://doi.org/10.1021/acs.langmuir.0c00635.

(9)     Craig, V. S. J.; Ninham, B. W.; Pashley, R. M. The Effect of Electrolytes on Bubble Coalescence in Water. *J. Phys. Chem.* **1993**, *97* (39), 10192–10197. https://doi.org/10.1021/j100141a047.

(10)     Chandran, P.; Bakshi, S.; Chatterjee, D. Study on the Characteristics of Hydrogen Bubble Formation and Its Transport during Electrolysis of Water. *Chem. Eng. Sci.* **2015**, *138*, 99–109. https://doi.org/10.1016/j.ces.2015.07.041.

(11)     Zhao, X.; Ren, H.; Luo, L. Gas Bubbles in Electrochemical Gas Evolution Reactions. *Langmuir* **2019**, *35* (16), 5392–5408. https://doi.org/10.1021/acs.langmuir.9b00119.

(12)     Chen, Q.; Wiedenroth, H. S.; German, S. R.; White, H. S. Electrochemical Nucleation of Stable N2 Nanobubbles at Pt Nanoelectrodes. *J. Am. Chem. Soc.* **2015**, *137* (37), 12064–12069. https://doi.org/10.1021/jacs.5b07147.

(13)     German, S. R.; Edwards, M. A.; Ren, H.; White, H. S. Critical Nuclei Size, Rate, and Activation Energy of H2 Gas Nucleation. *J. Am. Chem. Soc.* **2018**, *140* (11), 4047–4053. https://doi.org/10.1021/jacs.7b13457.

(14)    Perez Sirkin, Y. A.; Gadea, E. D.; Scherlis, D. A.; Molinero, V. Mechanisms of Nucleation and Stationary States of Electrochemically Generated Nanobubbles. *J. Am. Chem. Soc.* **2019**, *141*, 10801–10811. https://doi.org/10.1021/jacs.9b04479.

(15)    Hao, R.; Fan, Y.; Howard, M. D.; Vaughan, J. C.; Zhang, B. Imaging Nanobubble Nucleation and Hydrogen Spillover during Electrocatalytic Water Splitting. *Proc. Natl. Acad. Sci. U. S. A.* **2018**, *115* (23), 5878–5883. https://doi.org/10.1073/pnas.1800945115.

(16)    Battistel, A.; Dennison, C. R.; Lesch, A.; Girault, H. H. Local Study on Hydrogen and Hydrogen Gas Bubble Formation on a Platinum Electrode. *J. Phys. Chem. C* **2019**, *123* (17), 10849–10856. https://doi.org/10.1021/acs.jpcc.8b10920.

(17)    Chen, X.; Maljusch, A.; Rincón, R. A.; Battistel, A.; Bandarenka, A. S.; Schuhmann, W. Local Visualization of Catalytic Activity at Gas Evolving Electrodes Using Frequency-Dependent Scanning Electrochemical Microscopy. *Chem. Commun.* **2014**, *50* (87), 13250–13253. https://doi.org/10.1039/c4cc06100d.

(18)    Wang, Y.; Gordon, E.; Ren, H. Mapping the Nucleation of H2 Bubbles on Polycrystalline Pt via Scanning Electrochemical Cell Microscopy. *J. Phys. Chem. Lett.* **2019**, *10* (14), 3887–3892. https://doi.org/10.1021/acs.jpclett.9b01414.

(19)    Ando, K.; Uchimoto, Y.; Nakajima, T. Concentration Profile of Dissolved Gas during the Hydrogen Gas Evolution: An Optical Approach. *Chem. Commun.* **2020**, *56*, 14483–14486. https://doi.org/10.1039/d0cc05695b.

(20) Lasemi, N.; Pacher, U.; Zhigilei, L. V.; Bomatí-Miguel, O.; Lahoz, R.; Kautek, W. Pulsed Laser Ablation and Incubation of Nickel, Iron and Tungsten in Liquids and Air. *Appl. Surf. Sci.* **2018**, *433*, 772–779. https://doi.org/10.1016/j.apsusc.2017.10.082.

(21) Climent, V.; Coles, B. A.; Compton, R. G. Laser-Induced Potential Transients on a Au(111) Single-Crystal Electrode. Determination of the Potential of Maximum Entropy of Double-Layer Formation. *J. Phys. Chem. B* **2002**, *106* (20), 5258–5265. https://doi.org/10.1021/jp020054q.

(22) Fernández-Prini, R.; Alvarez, J. L.; Harvey, A. H. Henry's Constants and Vapor-Liquid Distribution Constants for Gaseous Solutes in H2O and D2O at High Temperatures. *J. Phys. Chem. Ref. Data* **2003**, *32* (2), 903–916. https://doi.org/10.1063/1.1564818.

(23) Li, D.; Beyer, C.; Bauer, S. A Unified Phase Equilibrium Model for Hydrogen Solubility and Solution Density. *Int. J. Hydrogen Energy* **2018**, *43* (1), 512–529. https://doi.org/10.1016/j.ijhydene.2017.07.228.

(24) Union, I.; Pure, O. F.; Chemistry, A. *Solubility Data Series*; 2014; Vol. 30. https://doi.org/10.1515/ci.2008.30.6.19.

(25) Epstein, P. S.; Plesset, M. S. On the Stability of Gas Bubbles in Liquid-Gas Solutions. *J. Chem. Phys.* **1950**, *18* (11), 1505–1509. https://doi.org/10.1063/1.1747520.

TOC Graphic